Adv. Manuf. (2022) 10:59–71
https://doi.org/10.1007/s40436-021-00374-x

Material removal at atomic and close-to-atomic scale by high-energy photon: a case study using atomistic-continuum method

Hao-Jie An[1] · Jin-Shi Wang[1] · Feng-Zhou Fang[1,2]

Received: 16 July 2021 / Revised: 5 September 2021 / Accepted: 15 September 2021 / Published online: 21 October 2021

Abstract Extreme ultraviolet (EUV) light plays an important role in various fields such as material characterization and semiconductor manufacturing. It is also a potential approach in material fabrication at atomic and close-to-atomic scales. However, the material removal mechanism has not yet been fully understood. This paper studies the interaction of a femtosecond EUV pulse with monocrystalline silicon using molecular dynamics (MD) coupled with a two-temperature model (TTM). The photoionization mechanism, an important process occurring at a short wavelength, is introduced to the simulation and the results are compared with those of the traditional model. Dynamical processes including photoionization, atom desorption, and laser-induced shockwave are discussed under various fluencies, and the possibility of single atomic layer removal is explored. Results show that photoionization and the corresponding bond breakage are the main reasons of atom desorption. The method developed can be further employed to investigate the interaction between high-energy photons and the material at moderate fluence.

✉ Jin-Shi Wang
jswang@tju.edu.cn

✉ Feng-Zhou Fang
fzfang@tju.edu.cn

[1] State Key Laboratory of Precision Measuring Technology and Instruments, Laboratory of MicroNano Manufacturing Technology (MNMT), Tianjin University, Tianjin 300072, People's Republic of China

[2] Centre of MicroNano Manufacturing Technology (MNMT-Dublin), School of Mechanical and Materials Engineering, University College Dublin, Dublin 4, Ireland

Keywords Extreme ultraviolet (EUV) · Molecular dynamics (MD) · Two-temperature model (TTM) · Photoionization · Atomic and close-to- atomic scale manufacturing (ACSM)

1 Introduction

The development of pulse laser technology has promoted the advancement of manufacturing technologies, improving the precision from macro- to micro- and even to nano-scales [1]. During the irradiation of the laser pulse, fast energy desorption mainly occurs on the focal position of ablated targets, which leads to a strong electronic excitation and shallow damage in target materials [2]. Having the characteristics of non-contact, high efficiency, and low damage, laser machining has become the main approach for various processes such as cutting and welding with high precision and surface quality [3].

The accuracy of laser machining has currently reached a nanometric level and has the potential to be developed toward atomic and close-to-atomic scale (ACS). Thus, a deep understanding of the material removal fundamentals and process is of great necessity. For semiconductors, the laser-material interaction process is influenced by the wavelength or photon energy. When the single-photon energy is smaller than the band gap, it is mainly absorbed via a multi-photon process. Otherwise, single-photon absorption dominates [4]. During laser irradiation, valence electrons that are excited by the pulse pass through the band gap become free, resulting in a high free-electron concentration in the surface layer. When the pulse width is at the sub-picosecond and femtosecond levels, photo-excited ionization may cause a non-thermal phase transition in semiconductors [5]. This means that the interaction

potential between atoms changes by the transient modification of interatomic bonding. A series of changes, including Coulomb explosion, spallation, evaporation, and ablation, may occur on the surface without a high temperature rise [1, 6].

Reducing the pulse width and wavelength are two possible ways to control the minimum material of laser machining. A short pulse can confine the energy deposition into the shallow surface layer and reduce the heat transfer to the subsurface region, which depresses the material damage. Laser damage in silicon can be reduced considerably when the pulse duration changes from nanoseconds to picoseconds [7]. Wavelength has an effect on the characteristics of ablation [8]. As the photon energy increases, the material can be removed by single-photon absorption, which increases the ionization level of the target atoms and consequently promotes the occurrence of a non-thermal process. The wavelength of laser machining has evolved from infrared [9], visible light to ultraviolet [10], and extreme ultraviolet (EUV) [11]. With the characteristics of high single-photon energy (generally exceeds several tens of eV [12]) and short photoelectron ranges, the EUV spectral region has a certain advantage in surface science [4]. A femtosecond EUV pulse has been generated by a free-electron laser, and the space- and time-resolved dynamics of thermal ablation on the nanometric scale can be studied based on newly informative time-resolved structural techniques [13, 14]. At present, there are some researches that have been related to the issue of material removal. For example, Stojanovic et al. [15] studied the material's response to a femtosecond EUV pulse using a free-electron laser and obtained an ablation crater at the micrometer level on the silicon's surface. Krzywinski et al. [16] stated that there were high charge state ions emitted from a Si target surface irradiated by sub-100 nm femtosecond pulses. Bravo et al. [2] studied the removal of polymethyl methacrylate photoresist irradiated by a 46.9 nm EUV laser pulse and obtained a hole with a depth as low as about 8 nm.

Although the experimental conditions are getting better controlled, it is still hard to conduct an effective study on the dynamic processes such as surface topography changes, ion emission, and atomic motion in such a short time through the experimental approach. However, this can be handled effectively using numerical simulation. The effective detection of surface topography changes and ion emission in the irradiation process is one of the difficulties in understanding the laser-material interaction mechanism. Molecular dynamics (MD) is a widely used numerical method that provides a deep understanding of the laser-material interaction at the atomic level, such as the instantaneous non-thermal phase transition, material desorption, photomechanical ablation, and defects induced by laser energy deposition, with the pulse duration from femtoseconds to nanoseconds [17]. During irradiation, the compress stress generated in the energy deposition zone and the shockwave propagating into the bulk target were observed, which resulted in the formation of voids in the subsurface followed by material removal [5]. For ultrashort laser pulse energy deposition, the MD method was coupled with a two-temperature model (TTM), which was also called the combined atomistic-continuum model [17]. This MD-TTM model was successfully used to study the microscopic mechanisms of femtosecond laser spallation and the ablation of metal [18, 19] and semiconductors [20].

Many laser processes are focused on nanometer-scale material removal. The question is whether the laser processes can be an efficient approach in atomic and close-to-atomic scale manufacturing (ACSM), which is the core competence of Manufacturing III [21–23]. As mentioned above, the ionization caused by short wavelengths is likely to be a necessary condition for removing material at atomic level. Experiments indicate that the material's behavior is more different under EUV irradiation than under longer wavelengths. For example, the study by Tanaka et al. [12] showed that the photoionized plasmas generated by EUV had a significant difference from that induced by an infrared laser pulse in angular distributions and energy spectra. Currently, the interaction mechanism of ultra-short EUV pulse, which is critical for developing ACSM, is unclear, and fundamental study using atomic/molecular simulation is necessary. However, the photoionization effect, an important feature in high-energy photon processes, is not explicitly considered in traditional MD-TTM method, which is addressed in this work. Here we propose a modified MD-TTM model handling the photoionization to investigate the femtosecond EUV irradiation on monocrystalline silicon under moderate fluence. The results show that the introduction of photoionization has an important influence on material removal behavior and is essential for studying the laser machining with high photon energy. In terms of the material removal depth and subsurface deformation, the EUV laser exhibits great potential to achieve ACSM.

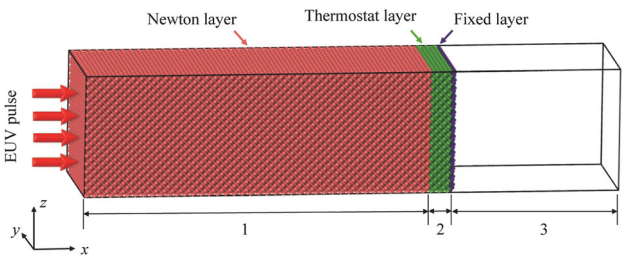

Fig. 1 Schematic diagram of MD-TTM model

2 Numerical approach

2.1 MD-TTM model

The EUV pulse in Fig. 1 is imposed on the (100) surface of the silicon target with a size of 24.3 nm × 8.2 nm × 8.2 nm. Considering the influence of long-wavelength phonons [25], a larger model that is 4 times longer is employed and the result shows that the influence of system size on the removal amount can be neglected. The periodic boundary condition is applied in the y and z dimensions. The model can be divided into two subsystems: the lattice subsystem represented by discrete MD particles and the electron subsystem treated as a continuum. Energy transportation is realized through the calculation of corresponding temperatures and heat conduction equations, as discussed below. The simulation domain is composed of three regions. In region one, the MD-TTM is employed to calculate the laser pulse energy deposition and the following photoionization and material removal are calculated through an inhomogeneous Langevin thermostat, which is applied to the local atoms divided by TTM grids. In region two, a 1.5 nm thick thermal layer is used to imitate the heat conduction from the lattice subsystem to the bulk by the Nose-Hoover thermostat of 300 K. The two layers of atoms are fixed to prevent the model from moving. According to the study conducted by Rutherford et al. [24], the electron grid was extended to region three so that the heat generated in the regions above could also be dissipated through the electron subsystem.

A three-dimensional grid with a size of 1.32 nm × 1.36 nm × 1.36 nm is employed to solve the diffusion equation of the electron temperature based on the finite difference method. To simulate the heat dissipation of electronic energy to the outside of the simulation unit, the electronic temperature is fixed at 300 K on the right side of region three [24]. In the MD-TTM part, each electron grid covers a group of lattice atoms, of which the temperature is calculated based on the equation below [18]

$$T_\mathrm{l} = \sum_{\mathrm{cell}} m_i |v_i - v_\mathrm{c}|^2 / (3k_\mathrm{B} N_\mathrm{cell}), \tag{1}$$

where m_i and v_i represent the mass and velocity of each atom, respectively, v_c the velocity of the mass center of the group, k_B the Boltzmann constant, and N_cell the number of atoms within the volumes of each electron cell. The temperature diffusion of both atomic and electron subsystems is solved by the TTM equations below

$$C_\mathrm{e}(T_\mathrm{e}) \frac{\partial T_\mathrm{e}}{\partial t} = \nabla (k_\mathrm{e}(T_\mathrm{e}, T_\mathrm{l}) \nabla T_\mathrm{e}) - G(T_\mathrm{e})(T_\mathrm{e} - T_\mathrm{l}) + S(x,t), \tag{2}$$

$$C_\mathrm{l}(T_\mathrm{l}) \frac{\partial T_\mathrm{l}}{\partial t} = \nabla (k_\mathrm{l}(T_\mathrm{l}) \nabla T_\mathrm{l}) + G(T_\mathrm{e})(T_\mathrm{e} - T_\mathrm{l}), \tag{3}$$

where C is the specific heat; k is the thermal conductivity; and the subscript e and l represents the electron and lattice subsystems, respectively. On the right side of Eq. (2), the first term corresponds to the energy exchange in the electron subsystem, which is determined by the lattice temperature (T_l), electronic temperature (T_e), and electronic thermal conductivity (k_e). The second term represents the energy exchange between the electron and lattice, where G is the electron-phonon coupling coefficient. The third term is the source term that represents the laser pulse. The electronic specific heat (C_e) is temperature dependent: $C_\mathrm{e} = \gamma T_\mathrm{e}$, where γ is 50 J/(m^3·K^2) according to the finite temperature density functional theory calculation [26]. The electron-phonon coupling coefficient is 2.8 × 10^{17} W/(m·K) according to density functional theory calculation [20] and the electronic thermal conductivity is the product of the electronic temperature and the electronic thermal diffusion coefficient (33.6 cm^2/s at room temperature) [24, 26]. It should be pointed out that Eq. (3) for the lattice subsystem is in fact not solved, because heat conduction is automatically accomplished for MD method. Therefore, it may not be necessary to assign the specific heat (C_l) and thermal conductivity (k_l) of the lattice.

A stable bulk silicon structure with 81 000 atoms is obtained by relaxing at 300 K and zero pressure for 10 ps. A 46.9 nm laser pulse of 100 fs is loaded along the x-direction corresponding to a direction perpendicular to the Si (100) surface. The interaction between the silicon atoms is calculated using the Stillinger-Weber potential [27], and the time step is set to 0.1 fs. Low fluencies ranging from 25 mJ/cm^2 to 100 mJ/cm^2 are performed to explore the cold removal mechanism. Each simulation is repeated three times to eliminate the impact of random errors.

2.2 Photoionization

In this study, photoionization is assumed to occur in the first fourteen atom layers on the top of the Si (100) surface. According to Beer's law, the energy absorption exhibits an exponential decrease along the depth direction, $I = I_0 \mathrm{e}^{-n_\mathrm{a}\sigma x}$, where n_a is the atom number density and σ is the atomic absorption coefficient. Correspondingly, the probability of an atom absorbing a photon is assumed to decrease exponentially along the depth direction. The schematic diagram of photoionization is shown in Fig. 2. For the EUV laser with a wavelength of 46.9 nm, the single-photon energy (26.44 eV) exceeds the work function of silicon (4.85 eV [28]). When a photon is absorbed, the silicon atom is marked as an ion. The photon energy subtracted by the work function is then converted to thermal

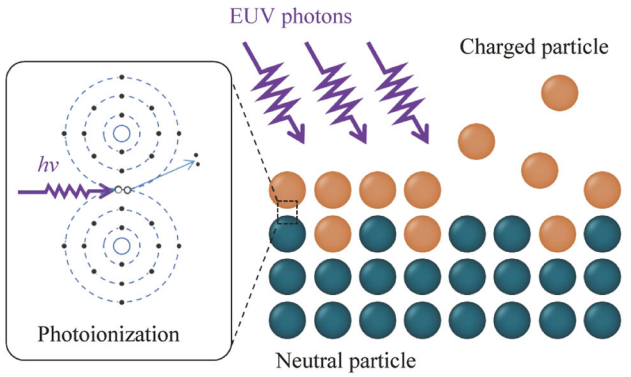

Fig. 2 Schematic diagram of photoionization (incident photon is absorbed by an atom with the emission of a photoelectron. The photoelectron energy which is equal to the photon energy minus the work function, is applied to the corresponding grid of electron subsystem)

energy and temperature, which are applied to the corresponding electron grid. After one photoionization event, both the ionization level and the charge of the ionized atom increase by one. The potential changes as the level of ionization increases. Because one silicon atom has four valence electrons, the atom is considered to be completely ionized when the ionization level reaches four. The bonds between this and its surrounding atoms are then broken by removing the attraction part of the potential function [28]. On the other hand, an ionized silicon atom may recombine with other electrons in the material, which is the so-called electron-ion recombination. When this occurs, the ionization level of the corresponding ion decreases by one until it returns to electric neutrality again. The average lifetime of ions is assumed to be 500 fs [28]. To this end, the effect of photoionization is integrated into the traditional MD-TTM model and the computation code is realized based on the large-scale atomic/molecular massively parallel simulator package [29]. Visualization and some analyses are performed using OVITO [30].

3 Results and discussion

3.1 Material removal and surface characterization

Figure 3 shows the morphology change of the bulk silicon that is irradiated by a 100 fs EUV pulse with a fluence of 100 mJ/cm^2. After the laser pulse is completed at 0.1 ps, no atom is immediately ejected from the surface. Some silicon atoms then begin to leave the surface. A total of 1 398 atoms are removed during the subsequent 100 ps. It can be inferred from the morphology image that the main cause is the vaporization of surface atoms. Following the removal process, the removed atoms gather together to form small clusters.

Figure 4a presents the evolution of the charge distribution of surface atoms. The ionization degree of these atoms decreases exponentially with depth, as predicted by Beer's law owing to the change in the probability of photon absorption along the depth direction. In the entire light-material interaction area, the average charge level of silicon atoms increases continuously during the irradiation process. At the end of the EUV pulse (100 fs), the average charge of each atom reaches a maximum of 3.85, corresponding to a photoionization level of about 2.49. This high charging state induces a strong Coulomb repulsion between the lattice atoms, which finally breaks the chemical bonds and leads to the removal of silicon atoms. The observed high charging state shows the influence of Coulomb repulsion on the atoms' removal, which is consistent with the experimental result where the removed silicon atoms with high charged states were recorded under EUV irradiation [16]. Figure 4b shows that the kinetic energy of the removed atoms ranges from 0 to 9 eV and has a maximum possibility near 0.9 eV. More than half of the removed atoms gain kinetic energy between 0.6 eV and 2.3 eV.

For the ACSM process, the material removal amount and surface integrity are two critical issues. Figure 5 plots the number of desorbed atoms and the lattice damage depth (thickness of the amorphous layer on top of the surface) under a 100 fs EUV pulse as a function of the fluence. In the range of 25–100 mJ/cm^2, both quantities increase with the laser fluence and have a turning point at 50–70 mJ/cm^2. At a fluence of 70 mJ/cm^2, about 174 silicon atoms are desorbed and removed from the target surface. When the laser fluence is less than 70 mJ/cm^2, the number of desorbed atoms increases with the fluence at a lower rate. When the laser fluence exceeds 70 mJ/cm^2, the rate at which the number of desorbed atoms increases with the increase of energy. The turning point corresponds to the threshold fluence, above which material removal occurs in the classical theory of laser machining. However, the results here imply that the so-called threshold fluence corresponds to the abrupt change of material removal rate. Below the threshold fluence, the material removal is very small. For example, it was reported that the weak surface changes introduced by low energy EUV were difficult to detect by traditional AFM, which could only be observed using optical or electron microscopy [12, 16]. However, the domain below the turning point should not be ignored at ACS and might be the key factor of high precision laser machining. A 5 nm removal depth was observed on silicon surface irradiated by 200 shots 46.9 nm laser pulse with an uneven intensity distribution at an average fluences of about 32 mJ/cm^2 in the work by Cui [31]. The undetected

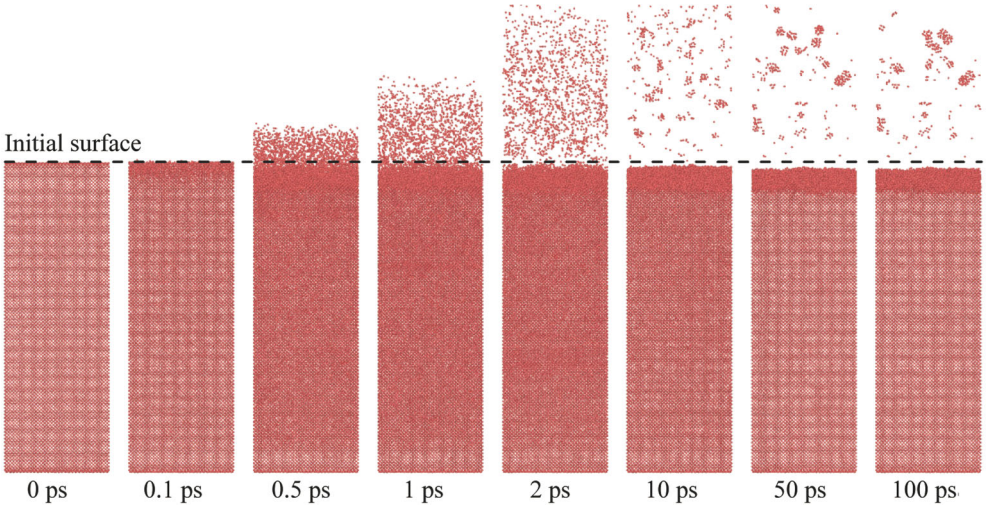

Fig. 3 Snapshots from an MD-TTM simulation with a laser fluence of 100 mJ/cm^2

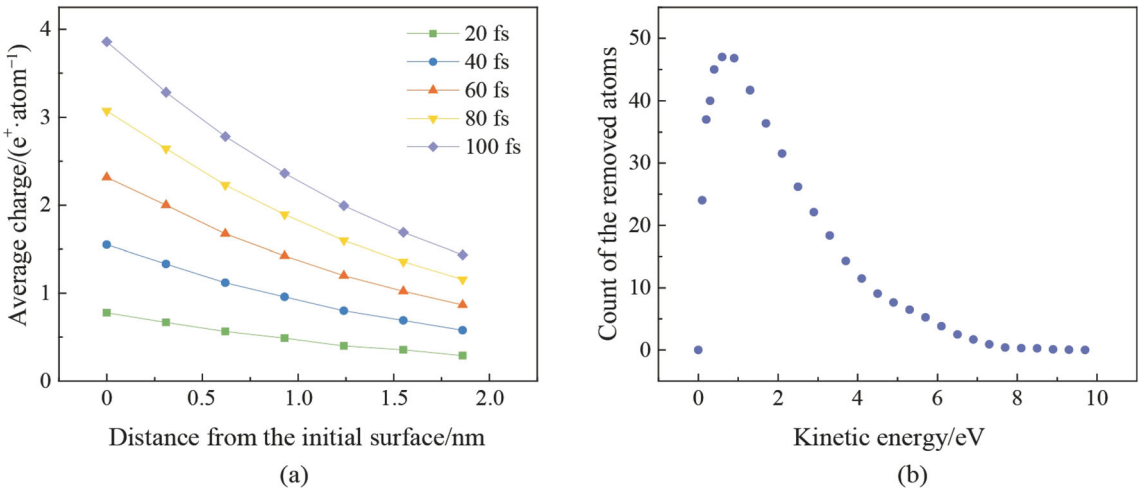

Fig. 4 Charge distribution and kinetic energy of the removed atoms **a** evolution of the average charge distribution of silicon atoms in the surface region under a fluence of 100 mJ/cm^2 (the time represents different moments during the laser pulse irradiation) and **b** kinetic energy distribution of the removed atoms at 2 ps

removal depth in the weak intensity area of the laser spot is expected to be the sub-nanometer level, which is similar to the value (about 0.5 nm at 100 mJ/cm^2) obtained in this work.

Figure 5b shows the variations of damage depth from the initial surface with laser fluence. The main technical index for measuring the damage depth is the thickness of the amorphous layer. It can be seen that the damage depth increases with increasing laser fluence. Figure 5c shows the MD snapshots of the irradiated surface at 100 ps under the EUV fluences of 50, 75 and 100 mJ/cm^2, respectively. The atoms are colored by the structure identification method for diamond lattices. For clarity, atoms with perfect cubic diamond structure are not shown. The result indicates that there is only an amorphous layer on the machined surface and the inner substrate maintains a high lattice integrity.

To explore the effect of laser irradiation on the surface morphology of materials, the 3D surface roughness parameters are used to characterize the surface topography. The 3D roughness parameters are calculated based on the full surface morphology of the region, which provides more surface information than the 2D parameters based on the line segment sample data. The contour arithmetic mean deviation (S_a) and mean square deviation (S_q) are performed to understand the surface characteristics of silicon after laser irradiation. S_a and S_q are defined as the functions of area (A) and height information (h) of the sample point [32]

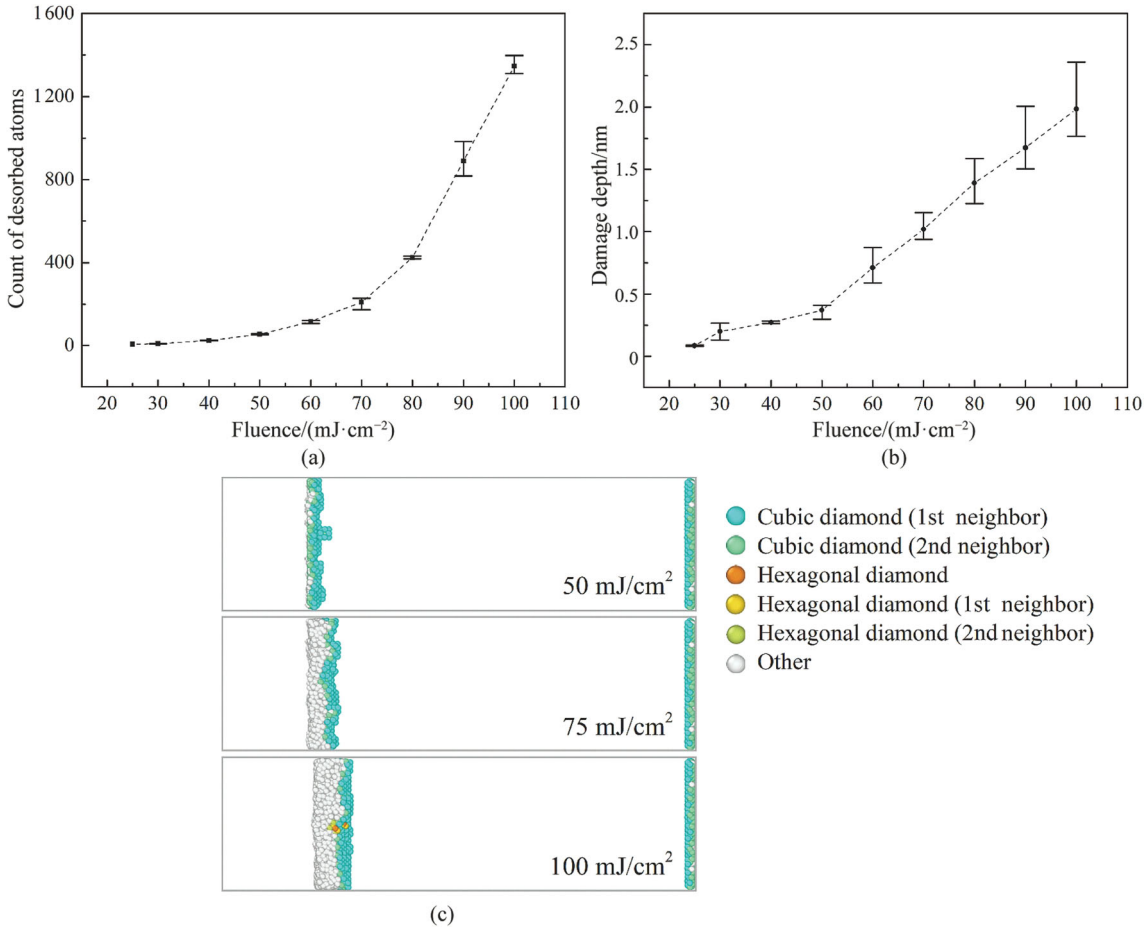

Fig. 5 Influence of laser fluence on the **a** number of desorbed atoms and **b** damage depth of processed surface, **c** MD snapshots of the lattice structure at 100 ps with three different laser fluences (the atoms are colored by the structure identification method for diamond lattices. For clarity, atoms that are considered to be the cubic diamond structure are not shown)

$$S_a = \frac{1}{A}\int |h| dA, \tag{4}$$

$$S_q = \sqrt{\frac{1}{A}\int h^2 dA}. \tag{5}$$

Figure 6a shows the variation of surface roughness S_a and S_q with the incident laser fluence, which shows an increasing trend when the fluence is below 70 mJ/cm^2. Meanwhile, when the laser fluence exceeds 70 mJ/cm^2, both the contour arithmetic mean deviation and mean square deviation reach a maximum value of about 0.09 nm and 0.11 nm, respectively. Compared with the quantities in Fig. 4, the roughness is not so sensitive to the fluence and has an asymptotic value, which also implies a threshold fluence near 70 mJ/cm^2. Below the threshold, the amount of removed atoms is relatively small and the surface is relatively flat. Above the energy threshold, the amount of removal increases rapidly with the increase of energy, and the surface roughness tends to a stable value. The result also shows that the roughness is on the atomic scale under all incident laser fluences, while the subsurface damage can reach the nanometer level at a high radiation dose and presents an increasing trend, as shown in Fig. 5b. This indicates that lattice integrity is a more stringent evaluation parameter than geometric accuracy. Figure 6b exhibits the details of the surface topography. At a fluence of 100 mJ/cm^2, the silicon surface exhibits some caves with a width of about 1 nm and a depth of about 1–3 atom layers. Both the number and size of caves and bumps are reduced with decreasing laser fluence. The silicon surface almost remains clean and flat at a laser fluence of 25 mJ/cm^2.

3.2 Shockwave and temperature field

During the interaction of the ultrafast laser pulse with the material, laser-induced compressive stress may appear in the subsurface of the irradiated target due to short pulse duration and fast energy deposition rate. Figure 7a shows the evolution of the internal stress distribution within the first 2 ps, which demonstrates the generation and

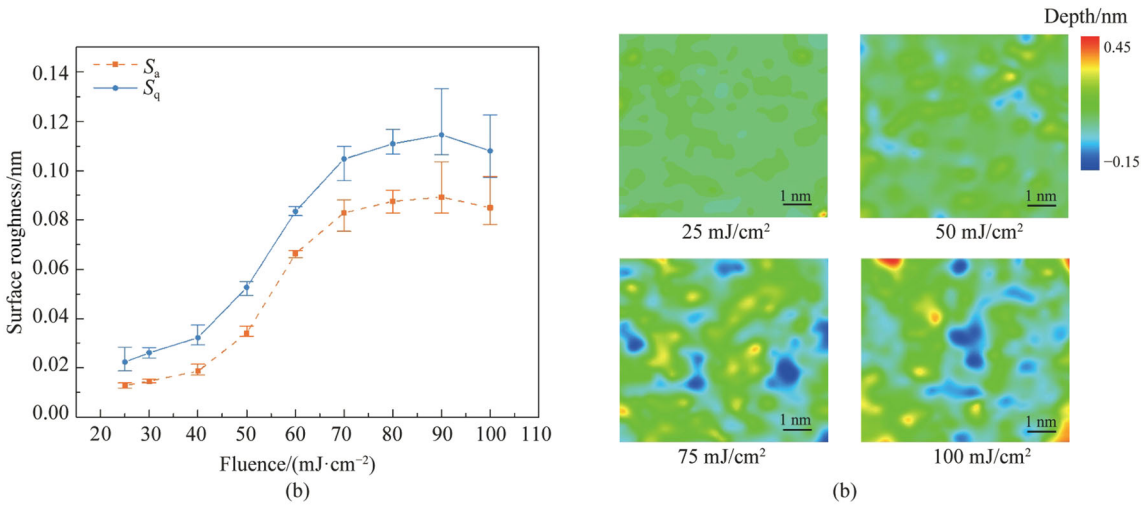

Fig. 6 Variation of surface topography **a** influence of laser fluence on surface roughness, **b** surface topography of silicon surface processed by different fluences

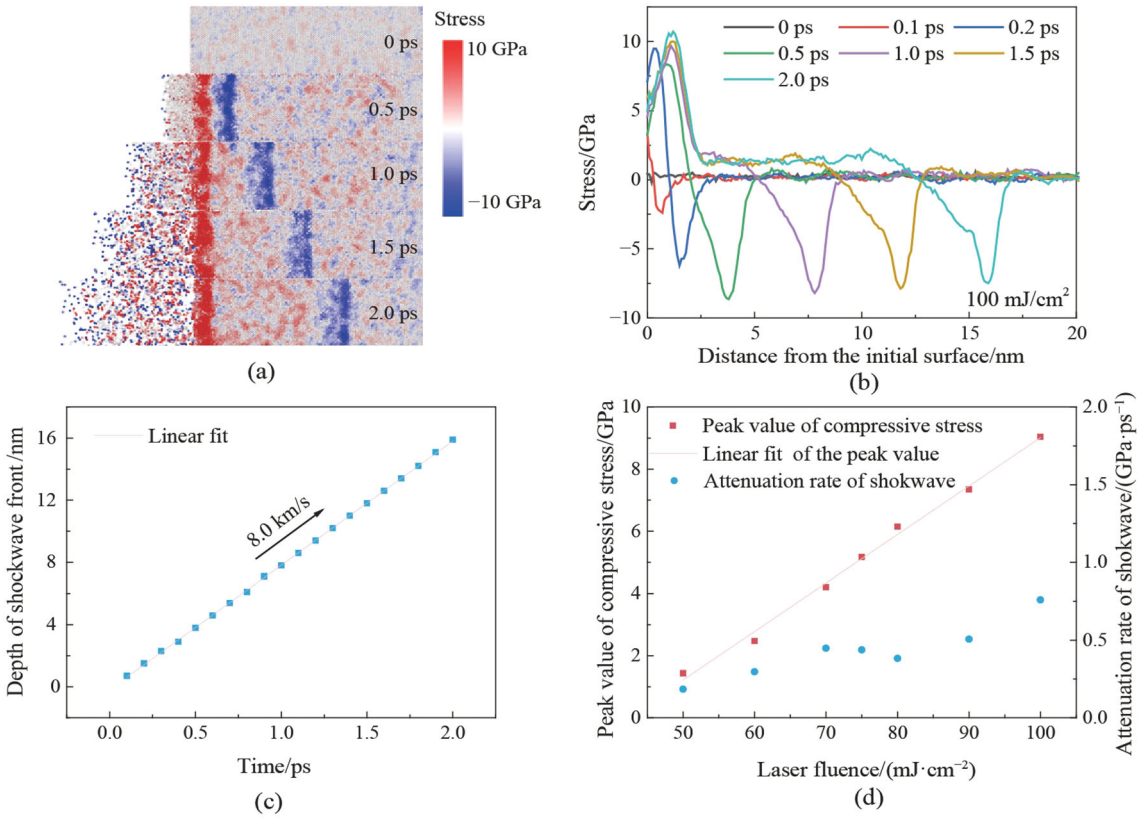

Fig. 7 Visual stress calculated for presenting the generation and propagation of the shockwave at a fluence of 100 mJ/cm^2 **a** map of stress predicted for laser irradiation, **b** distribution of stress along the laser's incident direction at different moments, **c** depth of compressive stress peak as a function of time, **d** variation of the peak value of compressive stress and the attenuation rate of the shockwave with laser fluence

propagation of a laser-induced shockwave at a fluence of 100 mJ/cm^2. The laser-induced compressive stress (blue atoms) occurs on the irradiated silicon subsurface and propagates into the target. Tensile stress (red atoms) mainly concentrates in the surface layer. Lattice structure analysis shows that when the stress wave passes through, some atoms will slightly deviate from the perfect cubic diamond structure. However, these temporary defects disappear at last, indicating only an elastic deformation in the

subsurface rather than the complex phase transformation or dislocation observed in previous studies [33–35].

Figure 7b shows the stress profile at various instants. Following the laser pulse, a tensile stress of about 10 GPa is generated at the position of the initial surface. The compressive stress increases and reaches the maximum (about 9.04 GPa) in 0.4 ps, which then begins to decay. After the shockwave passes, the residual tensile stress is observed with an average strength of about 1.35 GPa. As shown in Fig. 7c, the position of the compressive stress peak from the initial surface linearly increases with time, indicating a constant propagation speed at 8.0 km/s. Under different laser fluences, the average shockwave speed is about 7.83 km/s with a standard deviation of 0.08 km/s. It is noted that the sound speed along the [100] orientation of silicon is 8.43 km/s according to the elastic theory [36]. This indicates that the propagation of the laser-induced shockwave depends only on the material's properties rather than the fluence. The dependence of the maximum value and the attenuation rate of shockwave on the laser fluence are also calculated, as shown in Fig. 7d. A linear relationship between the maximum shockwave intensity and the fluence is observed with a slope of 0.156 GPa/(mJ·cm^{-2}). Besides the maximum value, the attenuation rate is also fluence-dependent. The higher is the fluence, the faster is the attenuation.

Figure 8a presents the evolution of the total energy of electronic and lattice subsystems. During the EUV pulse, the total energy of both the electronic and the lattice subsystems increase rapidly in the first 0.1 ps. The rapid increase of the electron energy to about 300 keV is due to the direct absorption of laser energy. At the same time, the lattice energy increases to – 322 eV following increase of the electron energy via the electron-phonon interaction. After irradiation, the electron energy begins to decrease and the lattice energy keeps increasing. At 0.58 ps, the lattice energy reaches its maximum, after which the energy transferred by the electronic to the lattice subsystem is less than the energy dissipated by the lattice subsystem to the interior.

The evolution and distribution of the electronic subsystem temperature (see Fig. 8b) show that the spatial distribution during laser irradiation is monotonous along the depth direction. The maximum electron temperature of about 60 000 K is detected in the initial surface at 0.1 ps, which is in the same order of magnitude as the value obtained in femtosecond laser ablation of silicon by carrier density model [37]. However, after laser irradiation, the temperature distribution tends to be flatter and the maximum temperature appears on the subsurface rather than the initial surface position. The reason for this phenomenon is that the system energy diffuses both into the bulk and to the external grid along with the thermal expansion of the material.

Figure 9 shows the heatmap of the lattice temperature under different fluencies. The overall lattice temperature increases due to the electron-phonon interaction and then decreases because of heat conduction by the thermal bath and electron grid. At the fluencies of 75 mJ/cm^2 and 100 mJ/cm^2, the effect of laser-induced shockwaves on the lattice temperature is observed clearly in Figs. 9c and d. In addition, the shockwave is reflected back to the surface after reaching the bottom, indicating that the Nose-Hoover thermostat is not sufficient to completely dissipate the shockwave. This will be handled in our future research.

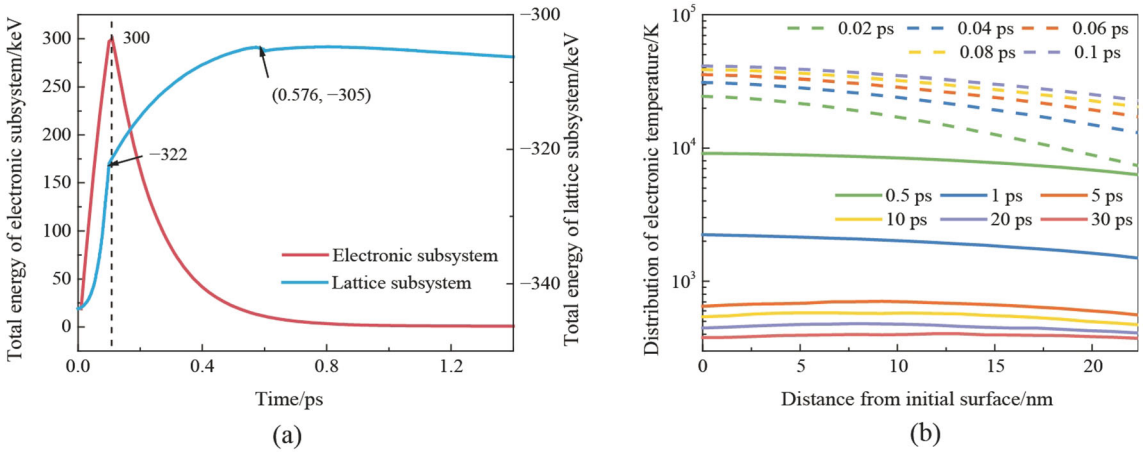

Fig. 8 Thermodynamic process of subsystems of silicon irradiated by a 100 fs laser pulse at a fluence of 100 mJ/cm^2 **a** evolution of the total energy of subsystems (the left side of the dashed line represents the laser pulse irradiation process) and **b** distribution of the electronic temperature along the laser incident direction (the dashed lines represent the laser pulse irradiation process, and the solid lines represent the process after laser pulse irradiation)

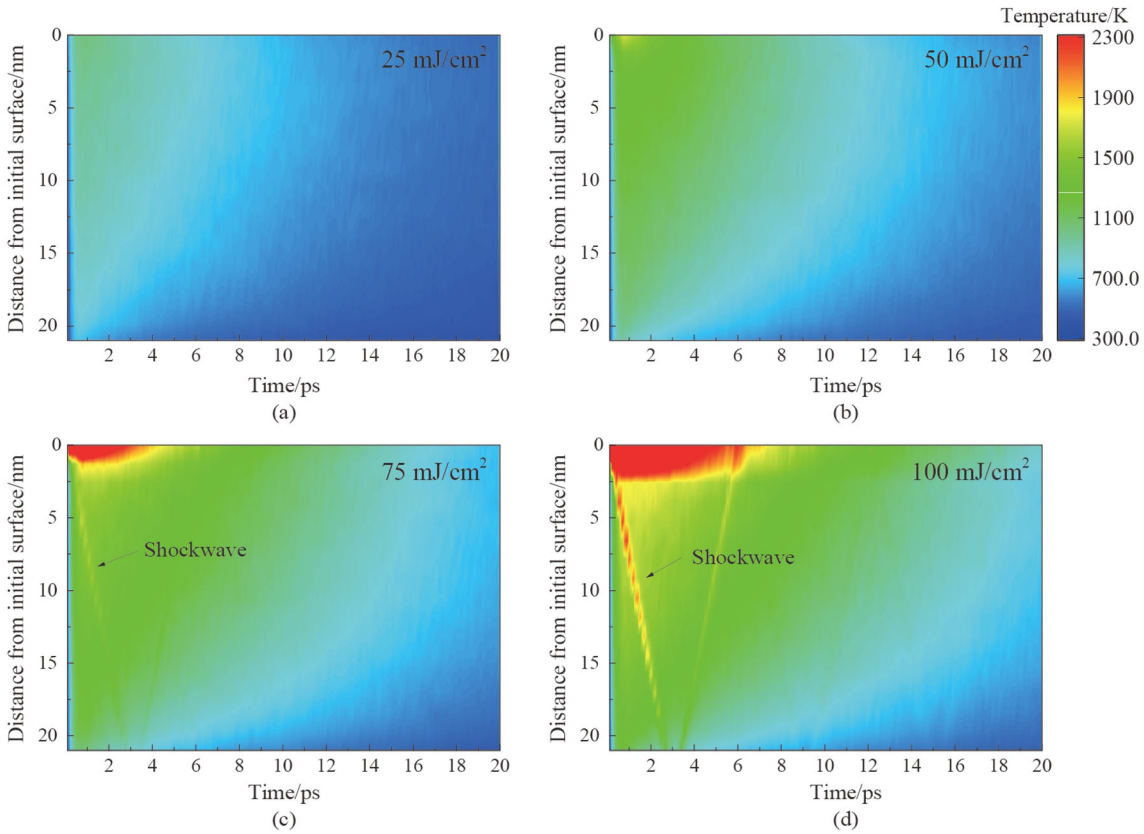

Fig. 9 Heatmaps showing changes in the lattice temperature of the silicon target irradiated by a 100 fs laser pulse at a fluence of **a** 25, **b** 50, **c** 75, and **d** 100 mJ/cm^2, respectively

3.3 Importance of photoionization on atomic layer removal

Material removal in the traditional MD-TTM model is a thermal process that happens above the threshold fluencies without the consideration of the photoionization mechanism [20, 38]. To verify this statement, simulations under the same conditions as above are conducted using the traditional MD-TTM. However, no material removal is observed. Therefore, the laser fluence is further improved to 8 J/cm^2. Figure 10 shows the corresponding material behavior. It can be seen that the surface layer is removed as a whole through the generation of cavities and high temperature vaporization. Lots of small cavities can be observed in the subsurface after 2 ps and merge into larger ones subsequently, completely destroying the surface.

In both traditional and modified MD-TTM models, laser energy is directly applied to the electronic subsystem. The irradiated energy is then transferred between two subsystems via electron-phonon coupling. However, the traditional MD-TTM model does not take the photoionization into account, so the pulse energy can only be converted into kinetic energy and potential energy of the lattice subsystem, resulting in only the thermodynamic phenomena appearing in the simulation process. The rapid deposition of energy in the surface area leads to material melting and the generation of compression stress, and some atoms are removed due to evaporation. On the other hand, tensile stress is generated at the subsurface due to the interaction of the compressive stress with the free surface [5]. Under the combined action of tensile stress and rapid energy deposition, cavities are generated and expand in the subsurface. In addition, material expansion at the solid-liquid interface also promotes the formation and expansion of cavities. Results show that the pure MD-TTM model mainly simulates the thermal ablation phenomenon of materials, which is suitable only for the calculation under high laser fluence or long pulse width, where the thermal effect dominates. In contrast, a very small removal and smooth surface can be achieved when the thermal effect is eliminated. The experiment by Thorstensen and Foss [7] showed that laser damage was reduced considerably with shorter pulse duration. Selective desorption of the chlorine/silicon surface was observed under the action of high-energy photons with almost no surface topography damage [39]. With short EUV pulses, the removal depth of only about 7.5 nm on PMMA was obtained by Bravo et al. [2]. This indicates the necessity to consider the photoionization

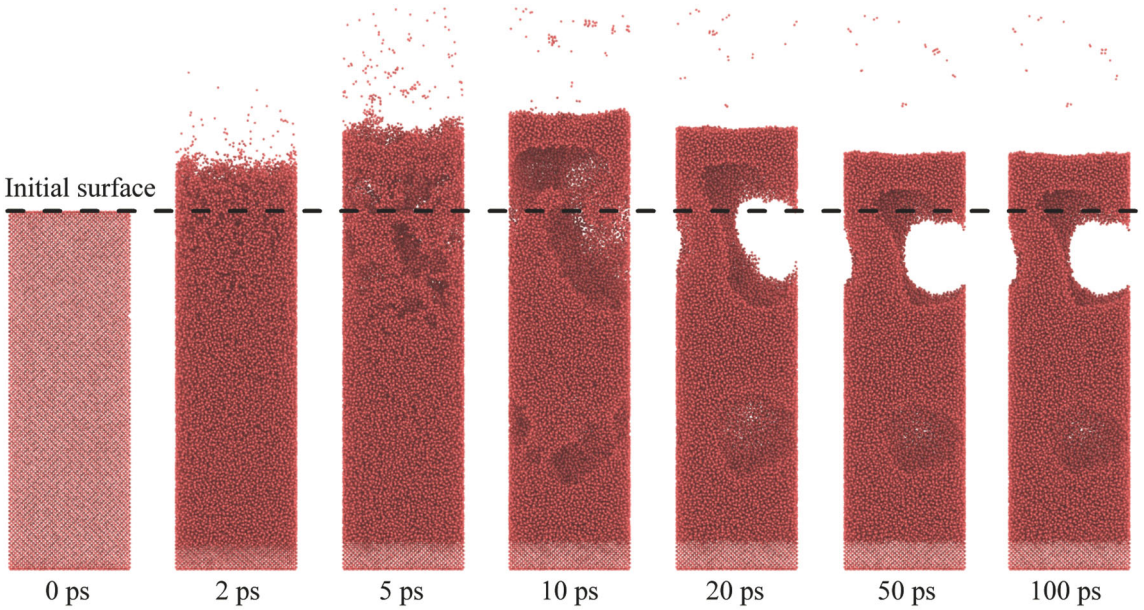

Fig. 10 Snapshots of silicon ablation using the traditional TTM-MD with a laser fluence of 8 J/cm^2

and chemical bond breaking in the atomic simulation of high energy photon and non-thermal processes [5], which is more concerned in this study.

A hybrid MD-TTM model combined with a photoionization mechanism presents an approach to describe the interaction mechanism between the materials and the laser. Existing experimental studies have illustrated the importance of the non-thermal process [5]. Hence, the thermodynamic process, photoionization, and chemical bond destruction caused by laser excitation are considered. The influence of wavelength is also reflected through the single-photon energy, which is not considered in the traditional model. Fast energy deposition leads to a highly ionized state on the surface, and atoms in the surface may be removed through the Coulomb force and chemical bond destruction. Calculation results show that under a low fluence, the thermal effect introduced by the laser is relatively small and dissipated in bulk silicon so that it will not cause damage to the target. The energy deposition of the ultrashort pulse laser also produces stress waves in the bulk silicon, which will affect the crystal lattice structure inside the block in the propagation process. However, at small laser fluence, the laser-induced stress is not enough to cause lattice damage after a shock wave has passed through. In short, the introduction of the photoionization mechanism makes the hybrid MD-TTM model more suitable for calculating the cold removal process below the ablation threshold.

The comparison between Fig. 3 and Fig. 10 evidently reveals that both the material removal amount and the surface damage can be significantly reduced by photoionization. It implies a potential approach for reaching the limit of subtractive manufacturing that removes only a few atomic layers with high controllability. For this reason, some tests are carried out using the modified MD-TTM to have preliminary knowledge on this issue. Here, only 100 atoms are excited randomly in the first few atomic layers. Figure 11 shows the corresponding snapshots. When photoionization occurs only at the first atomic layer, all the excited atoms are removed by the repulsive force exerted by each other and the atoms in the next layer. When photoionization occurs in more than one layer, some excited atoms stay on the surface and the removed atoms consist of not only the excited ones but also those not directly excited that mainly come from the first atom layer. When photoionization occurs in the first four layers, more excited atoms are confined in the surface, resulting in a smaller amount of removal.

Table 1 shows that both the surface damage depth and the number of amorphous atoms decrease as photoionization occurs within fewer atomic layers. Surface damage depth of about 1–2 atomic layers and a small surface roughness could be achieved if the photoionization was precisely controlled only to occur in the first layer. Therefore, it may be possible to realize the removal of a single atomic layer with negligible lattice damage. Some methods, including the extra atomic surface modification to reduce the binding energy [40], ion implantation to modify the surface, or the precise control of the laser to initially excite atoms with suspended bonds, may be helpful.

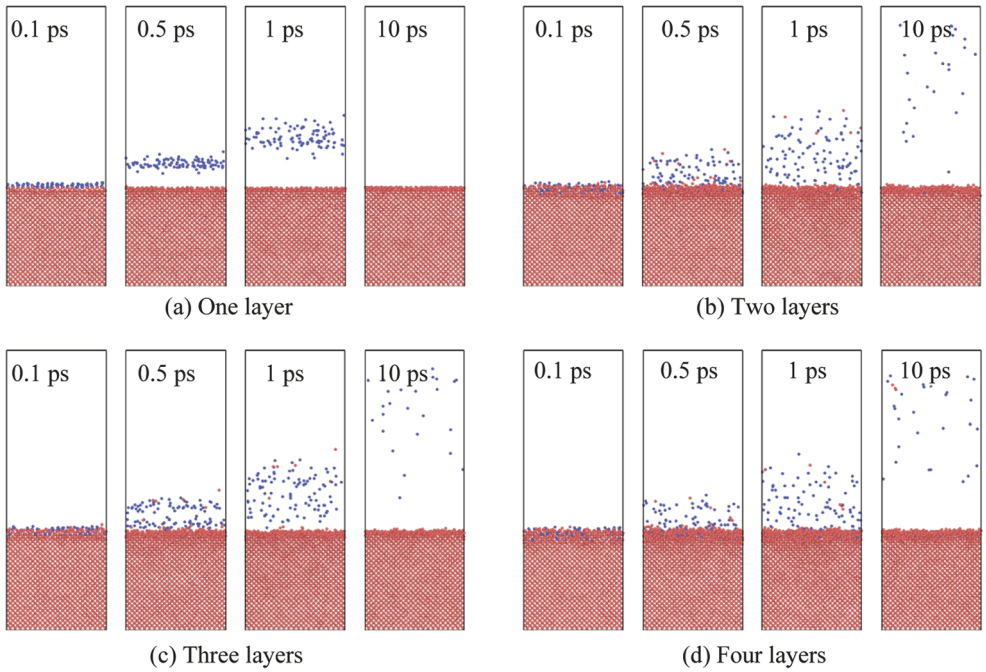

Fig. 11 Snapshots from modified MD-TTM simulations where 100 atoms are excited randomly in the first **a** one layer, **b** two layers, **c** three layers, and **d** four layers (blue particles represent the excited atoms)

Table 1 Simulation results where 100 atoms are excited randomly in the first few atomic layers

	Number of removed atoms	S_a /nm	Damage depth/nm	Number of amorphous atoms (#)
One layer	100	0.060	0.137	68
Two layers	106	0.081	0.258	131
Three layers	104	0.077	0.342	209
Four layers	89	0.080	0.432	326

4 Conclusions

Photoionization plays an important role in the interaction between the high-energy photon and the targeted material. In this study, a modified MD-TTM method considering the photoionization effect is proposed to investigate the material removal mechanism of silicon irradiated by a 46.9 nm EUV pulse with a duration of 100 fs, and the single atomic layer removal is explored. The main conclusions are drawn as follows.

(i) The absorption of the high-energy photon by a single atom in the modified model is realized through photoionization and increasing the energy of the corresponding electronic grid. The dynamic processes of several atomic layers' removal are then obtained.

(ii) At the laser fluence ranging from 25 to 100 mJ/cm^2, a theoretical precision of 46.9 nm laser machining can be achieved down to several atomic layers. Meanwhile, a threshold fluence of 70 mJ/cm^2 is detected, above which the number of desorbed atoms increases rapidly with the fluence.

(iii) Compressive stress waves are observed under the fluence above 50 mJ/cm^2. The shockwave reaches its maximum value within 0.4 ps, and then attenuates as it propagates into the material with a sound speed of about 7.83 km/s. Meanwhile, the attenuation rate is dependent on the laser fluence.

(iv) Compared with the traditional MD-TTM, the new approach introduces the direct interaction between high-energy photons and atoms, which makes it possible to study material removal at ACS under low fluence and lays a foundation for the further exploration of cold processing by a femtosecond EUV pulse.

Acknowledgments This study was supported financially by the National Natural Science Foundation (Grant No. 52035009) and the '111' project of the State Administration of Foreign Experts Affairs and the Ministry of Education of China (Grant No. B07014). Thanks to Shan Wu and Yan Xu for the discussions.

Reference

1. Guo B, Sun J, Hua Y et al (2020) Femtosecond laser micro/nano-manufacturing: theories, measurements, methods, and applications. Nanomanuf Metrol 3:26–67
2. Bravo H, Szapiro BT, Wachulak PW et al (2012) Demonstration of nanomachining with focused extreme ultraviolet laser beams. IEEE J Sel Top Quantum Electron 18:443–448
3. Joe DJ, Kim S, Park JH et al (2017) Laser-material interactions for flexible applications. Adv Mater 29(26):1606586. https://doi.org/10.1002/adma.201606586
4. Attwood D, Sakdinawat A (2017) X-rays and extreme ultraviolet radiation: principles and applications. Cambridge University Press, New York
5. Shugaev MV, Wu C, Armbruster O et al (2016) Fundamentals of ultrafast laser-material interaction. MRS Bull 41:960–968
6. Cui H, Zhao Y, Jiang S et al (2013) Experiment of Si target ablation with soft X-ray laser operating at a wavelength of 46.9 nm. Opt Laser Technol 46:20–24
7. Thorstensen J, Foss SE (2013) Investigation of depth of laser damage to silicon as function of wavelength and pulse duration. Energy Procedia 38:794–800
8. Juha L, Bittner M, Chvostova D et al (2005) XUV-laser induced ablation of PMMA with nano-, pico-, and femtosecond pulses. J Electron Spectrosc Relat Phenom 144/147:929–932
9. Ionin AA, Kudryashov SI, Seleznev LV et al (2013) Thermal melting and ablation of silicon by femtosecond laser radiation. J Exp Theor Phys 116:347–362
10. Shaheen M, Gagnon J, Fryer B (2019) Studies on laser ablation of silicon using near IR picosecond and deep UV nanosecond lasers. Opt Lasers Eng 119:18–25
11. Norman G, Starikov S, Stegailov V et al (2012) Nanomodification of gold surface by picosecond soft X-ray laser pulse. J Appl Phys 112:966–985
12. Tanaka N, Masuda M, Deguchi R et al (2015) Characterization of material ablation driven by laser generated intense extreme ultraviolet light. Appl Phys Lett 25(11):270. https://doi.org/10.1063/1.4930958
13. Carbone F, Baum P, Rudolf P et al (2008) Structural preablation dynamics of graphite observed by ultrafast electron crystallography. Phys Rev Lett 100(3):35501. https://doi.org/10.1103/PHYSREVLETT.100.035501
14. Sciaini G, Miller RJD (2011) Femtosecond electron diffraction: heralding the era of atomically resolved dynamics. Rep Prog Phys 74(9):96101–96136
15. Stojanovic N, von der Linde D, Sokolowski-Tinten K et al (2006) Ablation of solids using a femtosecond extreme ultraviolet free electron laser. Appl Phys Lett 89(24):241909. https://doi.org/10.1063/1.2405398
16. Krzywinski J, Sobierajski R, Jurek M et al (2007) Conductors, semiconductors, and insulators irradiated with short-wavelength free-electron laser. J Appl Phys 101(4):043107. https://doi.org/10.1063/1.2434989
17. Amouye FA, Förster DJ, Ghorbanfekr H et al (2021) Atomistic simulation of ultra-short pulsed laser ablation of metals with single and double pulses: an investigation of the re-deposition phenomenon. Appl Surf Sci 537:147775. https://doi.org/10.1016/j.apsusc.2020.147775
18. Wu C, Zhigilei LV (2014) Microscopic mechanisms of laser spallation and ablation of metal targets from large-scale molecular dynamics simulations. Appl Phys A 114:11–32
19. Wu C, Christensen MS, Savolainen JM et al (2015) Generation of subsurface voids and a nanocrystalline surface layer in femtosecond laser irradiation of a single-crystal Ag target. Phys Rev B 91(3):035413. https://doi.org/10.1103/PhysRevB.91.035413
20. Kan Z, Zhu Q, Ren H et al (2019) Femtosecond laser-induced thermal transport in silicon with liquid cooling bath. Materials 12(13):2043. https://doi.org/10.3390/ma12132043
21. Fang FZ, Zhang N, Guo D et al (2019) Towards atomic and close-to-atomic scale manufacturing. Int J Extreme Manuf 1:012001. https://doi.org/10.1088/2631-7990/ab0dfc
22. Fang FZ (2020) On atomic and close-to-atomic scale manufacturing-development trend of manufacturing technology. China Mech Eng 31:1009–1021
23. Mathew PT, Rodriguez BJ, Fang FZ (2020) Atomic and close-to-atomic scale manufacturing: A review on atomic layer removal methods using atomic force microscopy. Nanomanuf Metrol 16:1–20
24. Rutherford AM, Duffy DM (2007) The effect of electron–ion interactions on radiation damage simulations. J Phys Condens Matter 19(49):496201. https://doi.org/10.1088/0953-8984/19/49/496201
25. Xiong L, Chen Y, Beyerlein I et al (2021) Multiscale modeling of interface-mediated mechanical, thermal, and mass transport in heterogeneous materials: perspectives and applications. J Mater Res 36:2601–2614
26. Khara GS, Murphy ST, Daraszewicz SL et al (2016) The influence of the electronic specific heat on swift heavy ion irradiation simulations of silicon. J Phys Condens Matter 28:395201. https://doi.org/10.1088/0953-8984/28/39/395201
27. Stillinger FH, Weber TA (1985) Computer simulation of local order in condensed phases of silicon. Phys Rev B 31:5262. https://doi.org/10.1103/PhysRevB.31.5262
28. Herrmann RFW, Gerlach J, Campbell EEB (1988) Ultrashort pulse laser ablation of silicon: an MD simulation study. Appl Phys A 66(1):35–42
29. Plimpton S (1955) Fast parallel algorithms for short-range molecular dynamics. J Comput Phys 117:1–19
30. Stukowski A (2010) Visualization and analysis of atomistic simulation data with OVITO: the open visualization tool. Modell Simul Mater Sci Eng 18:015012
31. Cui HY (2018) Research on interaction of capillary discharge 46.9 nm laser with solid targets. Dissertation, Harbin Institute of Technology
32. Li Y, Shuai M, Zhang J et al (2018) Molecular dynamics investigation of residual stress and surface roughness of cerium under diamond cutting. Micromachines 9(8):386. https://doi.org/10.3390/mi9080386
33. Levitas VI, Chen H, Xiong L (2017) Lattice instability during phase transformations under multiaxial stress: modified transformation work criterion. Phys Rev B 96(5):054118. https://doi.org/10.1103/PhysRevB.96.054118
34. Levitas VI, Chen H, Xiong L (2017) Triaxial-stress-induced homogeneous hysteresis-free first-order phase transformations with stable intermediate phases. Phys Rev Lett 118(2):025701. https://doi.org/10.1103/PhysRevLett.118.025701
35. Chen H, Levitas VI, Xiong L (2019) Amorphization induced by 60° shuffle dislocation pileup against different grain boundaries in silicon bicrystal under shear. Acta Mater 179:287–295
36. Watanabe K, Ishizaka Y, Ohmura E et al (2000) Analysis of laser ablation process in semiconductor due to ultrashort-pulsed laser with molecular dynamics simulation. Proc SPIE Int Soc Opt Eng 3933:46–55

37. Wan DP, Wang J, Mathew P (2011) Energy deposition and non-thermal ablation in femtosecond laser grooving of silicon. Mach Sci Technol 15:263–283
38. Norman GE, Starikov SV, Stegailov VV (2012) Atomistic simulation of laser ablation of gold: effect of electronic pressure. J Exp Theor Phys 114(5):792–800
39. Amasuga H, Nakamura M, Mera Y et al (2002) The atomic processes of ultraviolet laser-induced etching of chlorinated silicon (1 1 1) surface. Appl Surf Sci 197/198:577–580
40. Yajima A, Nakamura Y, Mera Y et al (2005) STM observations of photo-induced jumps of chlorine atoms chemisorbed on Si(111)-(7×7) surface. Surf Sci 593(1/3):155–160

Hao-Jie An is a Ph.D. candidate studying at the Laboratory of Micro/Nano Manufacturing Technology (MNMT), Tianjin University. His research interests focus on the material removal at the atomic and close-to-atomic scale.

Jin-Shi Wang is a post-doctoral researcher working at the Laboratory of Micro/Nano Manufacturing Technology (MNMT), Tianjin University. His research focuses on nanometric machining and atomic and close-to-atomic scale manufacturing (ACSM).

Feng-Zhou Fang is a joint professor working at both Tianjin University and University College Dublin. His research focuses on both fundamental studies and application development in the areas of micro/nano machining, optical freeform design and manufacturing, ultra-precision machining and measurement, and ACSM benefiting a variety of industries in medical devices, bio-implants, optics and molds sectors.